

An Investigation of Polymeric Nanocomposite: Surface Functionalization and Nanofiller Effect

Zhanhu Guo¹, Xiaofeng Liang¹, Brian Shedd¹, Roberto Scaffaro^{1,2} and H. Thomas Hahn¹,

(1) Multifunctional Composite Lab, Mechanical & Aerospace Engineering Department,
University of California at Los Angeles, Los Angeles, CA 90095

(2) Department of Chemical Engineering and Materials, University of Palermo, Viale delle
Scienze, Ed. 6, Palermo, 90128, Italy

1. Introduction

Transition metal oxide such as copper (I and II), iron (II and III) and zinc oxide nanomaterials have special physicochemical properties arising from the quantum size effect and high specific surface area, which may be different from their atomic or bulk counterparts. Polymeric nanocomposite embedded with the above nanoparticles (NPs) have attracted much interest due to their high homogeneity, flexible processability and tunable physical such as mechanical, magnetic, optical, electric and electronic properties.¹⁻⁵ Furthermore, cheap ceramic nanoparticles within the polymeric matrix render the nanocomposite potential electronic device applications such as the photovoltaic (solar) cell⁶ and the magnetic data storage; the functional groups of the polymer surrounding the nanoparticles enable these nanocomposites suitable for variable applications such as site-specific molecule targeting application in the biomedical areas.

The *ex-situ* methods, *i.e.* by dispersing the synthesized nanoparticles into organic polymeric solution⁷⁻⁹ and *in-situ* monomer polymerization methods in the presence of the nanoparticles¹⁰⁻¹² have been reported for polymeric composite fabrication. The interactions between the polymer and the nanoparticles for the *ex-situ* formed mixtures are normally steric interaction forces, van der Waals forces, or Lewis acid-base interactions; however, *in-situ* forming methods can create strong chemical bonding within the nanocomposites, which is expected to produce a more-stable and higher-quality nanocomposite. The interfacial interaction between the nanofillers and the polymer matrix plays a crucial role in determining the quality and properties of the nanocomposite. Poor linkage between the filler and the polymer matrix will introduce artificial defects such as voids, which consequently have a deleterious effect on the mechanical properties of the nanocomposite.¹³ Introducing good bond between the nanoparticles and the polymer matrix is still a challenge for specific composite fabrication. However, appropriately chemical engineering treatment (functionalization) of nanofiller surface by introducing proper functional groups could improve both the strength and toughness of the composites with the improved compatibility between the nanofillers and the polymer matrix.

In this project, vinyl ester resin, as a thermosetting polymer matrix possessing high mechanical properties and superior resistance to moistures and chemicals has been successfully used to fabricate high-quality particulate nanocomposites filled with alumina, zinc oxide, or copper oxide nanoparticles, respectively. The effect of the bi-functional coupling agent, methacryloxypropyl-trimethoxysilane (MPS), on the *in-situ* free radically polymerized vinyl ester resin nanocomposite in the presence of ceramic nanoparticles was investigated. FT-IR and TGA data analysis indicated that MPS was covalently bound onto the nanoparticle surface. The nanocomposites containing the functionalized nanoparticles showed improved tensile strength as compared with the nanocomposites formed with the unmodified nanoparticles.

2. Experimental

2.1 Surface Functionalization of Nanoparticles

The nanoparticle functionalization follows the procedures similar to our recently reported alumina nanoparticle functionalization¹⁴ and is described briefly here. Nanoparticles were added into a mixture of MPS and THF. The resulting colloidal suspension was ultrasonically stirred for one hour and precipitated by sedimentation at room temperature. The precipitated nanoparticles were rinsed with THF to remove the excessive MPS and dried completely in a vacuum oven at room temperature to remove the solvent.

2.2 Nanocomposite Fabrication

The as-received nanoparticles or MPS functionalized nanoparticles were dispersed into 30 ml resin. The dispersion was carried out in an ice-water ultrasonic bath for about 1 hour. The nanoparticle/ resin solution was placed into an 85 °C oven for 15 minutes in vacuum to remove gases and ensure good dispersion quality. The above solution was then ultrasonically stirred in an ice-water ultrasonic bath until the temperature cooled down. Then 2.0 wt% catalyst (initiator) was added into the nanoparticle/resin solution, which was stirred and degassed for 2 minutes. 0.3 wt% promoter was added and mixed quickly. The mixed viscous solution was poured into various silicone rubber molds. The curing via free-radical bulk co-polymerization or homopolymerization initiated by the catalyst was done at room temperature for half hour followed by postcuring at 85 °C for 1 hour under normal atmospheric conditions and cooled down to room temperature naturally in the oven.

2.3 Characterization

A Fourier transform infrared (FT-IR) spectrometer (Jasco, FT-IR 420) in transmission mode under dried nitrogen flow (10 cubic centimeters per minute, ccpm) was used to test the physicochemical interaction between MPS and nanoparticles. The liquid MPS dispersant was mixed with powder KBr, ground and compressed into a pellet. Its spectrum was recorded as a reference to be compared with that of the MPS functionalized nanoparticles.

Thermo-gravimetric analysis (TGA, PerkinElmer) was conducted on the as-received and MPS-treated nanoparticles from 25 °C to 600 °C with an argon flow rate of 50 ccpm and a heating rate of 10 °C/min. Thermal degradation of the nanocomposites with different nanoparticle loadings was studied by TGA with procedures similar to nanoparticles.

Atomic force microscope (AFM) (Digital instruments, multimode) was utilized to characterize the morphology (size and shape) of the as-received and MPS treated nanoparticles operated in tapping mode. The samples were prepared by dispersing the nanoparticles in ethanol under ultrasonic stirring, dropping some of the solution on a glass slide, and evaporating the solvent naturally. The dispersion quality of the nanoparticle within the vinyl ester resin matrix was investigated by AFM and SEM (scanning electron microscope, JEOL field emission scanning electron microscope, JSM-6700F) on the cross-section area of the polished nanocomposite. The SEM specimens were prepared by sputter coating a thin gold layer with a thickness about 3 nm on the polished nanocomposite sample.

Optical absorption of the nanocomposite was measured in a UV-VIS-NIR scanning spectrophotometer (Mode: UV-310PC). Steady-state photoluminescent emission property was measured in an Ocean Optics system, exciting with a home-made lamp using an inorganic light emitting diode (LED) with an excitation wavelength of 365 nm. A long wavelength pass filter was used to cut off the emission lower than 380 nm to remove the reflection effect.

Optical absorption and photon-excited luminescence were recorded in a nanocomposite thin film with a thickness of about 300 micrometers and the samples were prepared by polishing the composites with 4000 grit sand paper, then with 50 nm alumina particles. All experiments were conducted at room temperature.

The tensile strength and Young's modulus of the fabricated nanocomposites were evaluated by microtensile tests following the American Society for Testing and Materials (ASTM, 2005, standard D 1708-02a) using an Instron 5544 testing machine. A crosshead speed of 0.15 mm/min was used and strain (mm/mm) was calculated by dividing the crosshead displacement (mm) by the gage length (mm). The fracture surface was then studied by bright field optical microscope (OM, Olympus TH4-100) and SEM.

3. Results and discussion

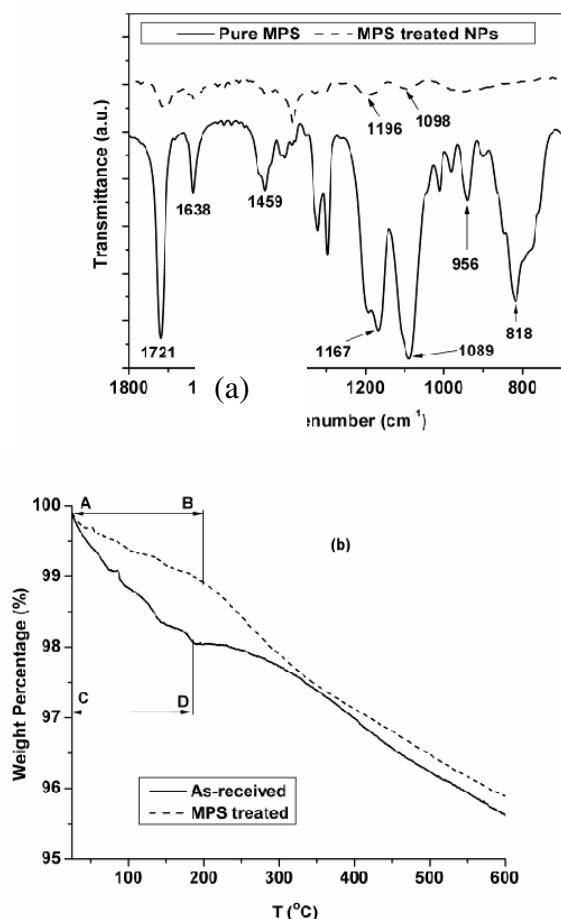
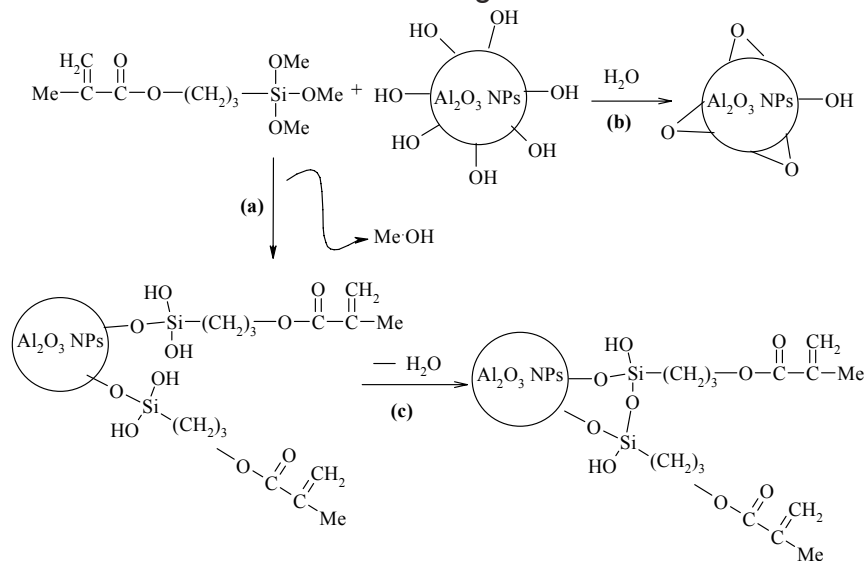


Fig. 1 (a) FT-IR spectra of pure MPS and MPS-treated nanoparticles; (b) TGA of the as-received nanoparticles and the MPS functionalized nanoparticles.

Fig. 1(a) shows FT-IR spectra of pure MPS and MPS-functionalized nanoparticles. The characteristic peaks at 818 cm^{-1} , 1089 cm^{-1} , and 1638 cm^{-1} are due to $-\text{Si}-\text{OCH}_3$, Si-O and C=C vibration of MPS, respectively. The peaks at 1721 cm^{-1} and 1167 cm^{-1} are due to the C=O and C-O vibration, respectively. The disappearance of the peak at 818 cm^{-1} characteristic of $-\text{Si}-\text{OCH}_3$ and the presence of other peaks characteristic of MPS in the MPS treated nanoparticles indicate the successful functionalization of nanoparticles with MPS. Thermogravimetric analysis of the as-received alumina nanoparticles shows the existence of

both moisture by physical adsorption and hydroxyl groups by chemical bonding in Fig. 1(b). Within the temperature range C–D, the weight loss is from evaporation of the physically adsorbed moisture. Beyond D, dehydration of chemically adsorbed water leads to weight loss. The scheme of the reaction is shown in following.



Scheme of (a) alumina nanoparticle functionalization with MPS, (b) dehydration of hydrolyzed alumina nanoparticles, c) condensation of hydrolyzed MPS

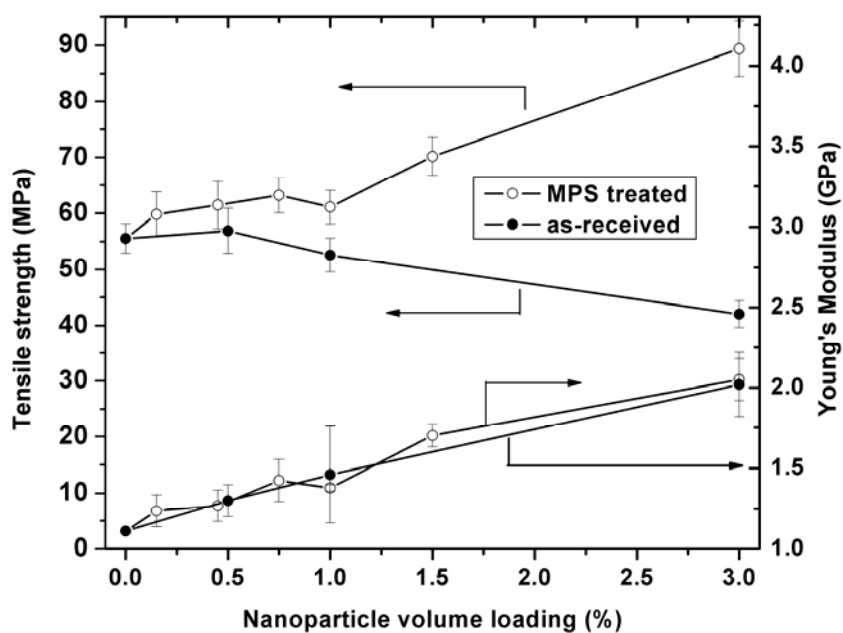


Fig.2 Tensile strength and Young's Modulus as a function of alumina nanoparticle loading.

Fig. 2 shows the effect of alumina particle loading on the mechanical properties, which indicates the good interfacial interaction between the nanoparticle and the polymeric matrix after the particle surface treated. Similar mechanical properties were observed in the zinc

oxide and copper oxide composites. Fig. 3 shows the PL property as a function of the zinc oxide particle loading. After functionalization, the PL intensity increased due to the better distribution of the nanoparticle in the polymeric matrix.

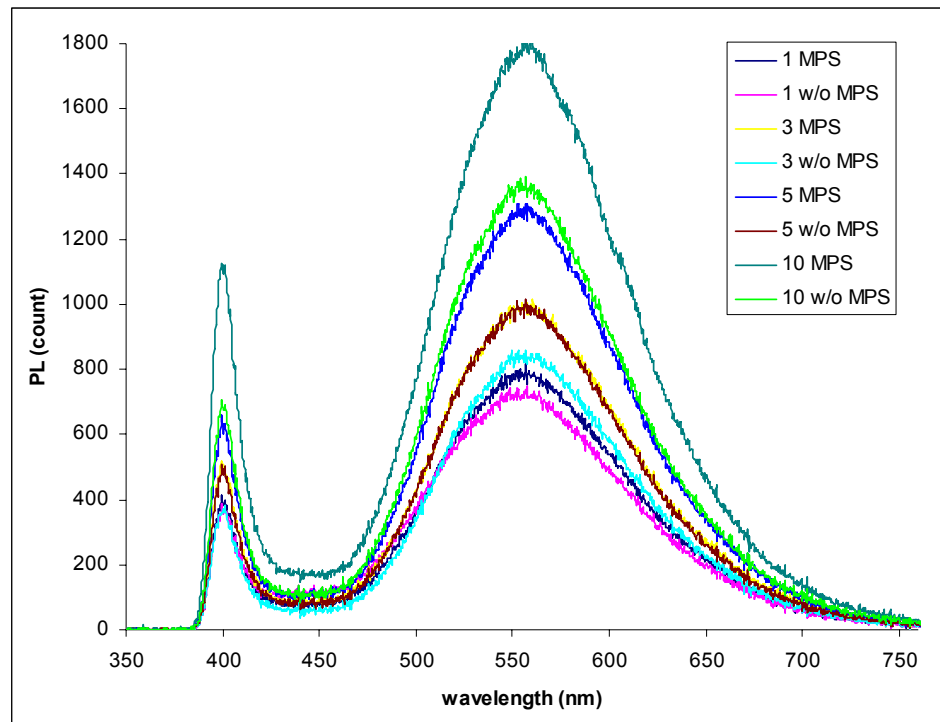
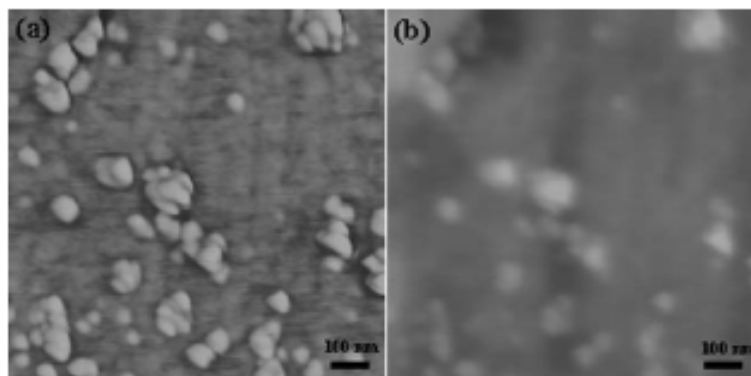


Fig. 3 PL graphs of ZnO/vinyl resin nanocomposite

The particles were observed to be agglomerated and poorly linked with polymer in the as-received particle filled composite shown in Fig. 4 (a, b). However, the functionalized particles dispersed more uniform and no air gap was observed in the composite shown in Fig. 4 (c, d). The improved particle distribution and the strong bonds are responsible for the improved mechanical properties and the enhanced photoluminescent properties.



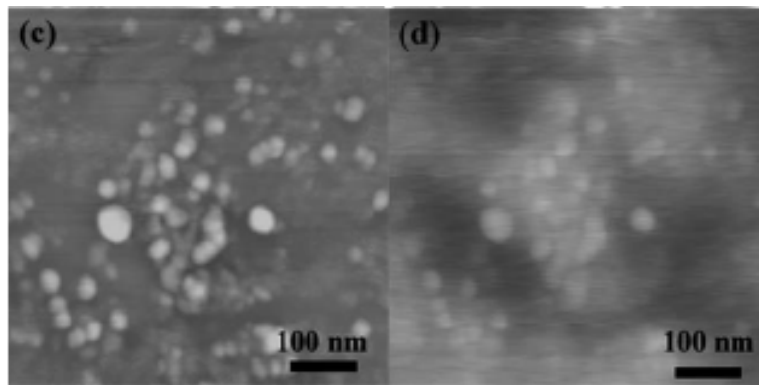


Fig.4 (a) (c) phase images, and (b) (d) height image of the cross-section of the nanocomposite for the functionalized NPs and as-received NPs.

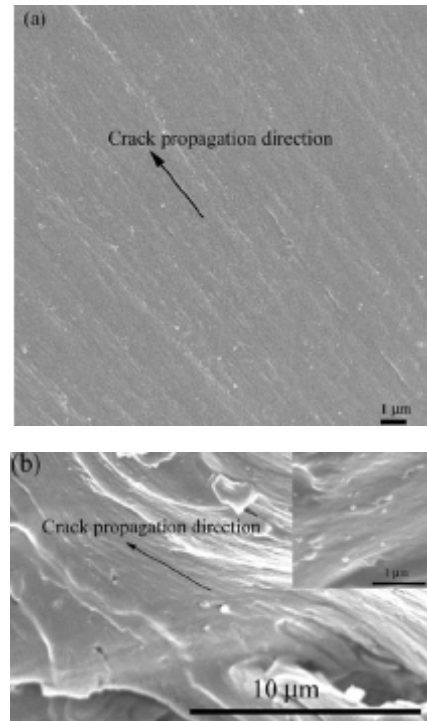


Fig.5 SEM micrographs of (a) the cured pure resin and (b) the nanocomposite with 3 vol% functionalized nanoparticle filling (inset in (b) shows the enlarged fracture surface with NPs).

Figures 5 (a) and (b) are SEM micrographs of fracture surfaces for neat resin and 3 v% nanocomposite. Even at the micron scale, the neat resin shows a smooth fracture surface while the nanocomposite shows a rough fracture surface. This micro-rough structure can be attributed to the matrix shear yielding or local polymer deformation between the nanoparticles rather than the intra-particle propagating cracks due to the difficulty in breaking the alumina nanoparticle arising from the high hardness¹⁵ as compared with the resin matrix. The enlarged SEM image (the inset of Figure 5 (b)) showing the protruded nanoparticles also indicates that the cracks pass around the nanoparticle without damaging it, which was also observed in $\text{Al}_2\text{O}_3/\text{CaSiO}_3$ filled epoxy nanocomposites.¹⁵ The protruded nanoparticles seen on the nanocomposite surface are observed to be covered with the matrix polymer, indicating the

presence of good adhesion between the nanoparticle and the polymer matrix through the chemical bonding.¹³

Conclusion

Vinyl ester resin nanocomposites filled with unmodified and MPS-modified ceramic nanoparticles were fabricated and the effect of the MPS on the subsequent physicochemical (thermal, optical and photoluminescent) properties was investigated. Strengthening effect of the nanocomposite was attributed to the surface functionalization. Increased photoluminescence property was observed in the MPS modified ZnO nanoparticle filled nanocomposite. Both the larger surface area and the increased oxygen vacancy are responsible for the enhanced photoluminescence property. In addition, the introduction of MPS onto nanoparticle surface has partially increased the thermal resistance to degrade as observed in TGA.

Acknowledgement

This project is supported by the Air Force Office of Scientific Research through AFOSR Grant FA9550-05-1-0138 managed by Dr. B. Les Lee.

References

- 1 C. Castro, J. Ramos, A. Millan, J. G. Calbet, and F. Palacio, *Chem. Mater.*, **12**, 3681 (2000).
- 2 V. Yong and H. T. Hahn, *Nanotechnology*, **15**, 1338 (2004).
- 3 J. J. Mack, L. M. Viculis, A. Ali, R. Luoh, G. Yang, H. T. Hahn, F. K. Ko, and R. B. Kaner, *Adv. Mater.*, **17**, 77 (2005).
- 4 G. Sandi, H. Joachin, R. Kizilel, S. Seifert, and K. A. Carrado, *Chem. Mater.*, **15**, 838 (2003).
- 5 Z. Guo, L. L. Henry, V. Palshin, and E. J. Podlaha, *J. Mater. Chem.*, **16**, 1772 (2006).
- 6 W. J. E. Beek, M. M. Wienk, and R. A. J. Jassen, *Adv. Mater.*, **16**, 1009 (2004).
- 7 F. Mammeri, E. Le Bourhis, L. Rozes, and C. Sanchez, *J. Mater. Chem.*, **15**, 3787 (2005).
- 8 C. Sanchez and F. Ribot, *New J. Chem.*, **18**, 1007 (1994).
- 9 P. Judeinstein and C. Sanchez, *J. Mater. Chem.*, **6**, 511 (1996).
- 10 E. Marutani, S. Yamamoto, T. Ninjbadgar, Y. Tsujii, T. Fukuda, and M. Takano, *Polymer*, **45**, 2231 (2004).
- 11 X. Xu, G. Friedman, K. Humfeld, S. Majetich, and S. Asher, *Chem. Mater.*, **14**, 1249 (2002).
- 12 S. Yu and G. M. Chow, *J. Mater. Chem.*, **14**, 2781 (2004).
- 13 X. Zhang and L. C. Simon, *Macromolecular Materials and Engineering*, **290**, 573 (2005).
- 14 Z. Guo, T. Pierce, O. Choi, Y. Wang, and H. T. Hahn, *J. Mater. Chem.*, **16**, 2800 (2006).
- 15 B. Wetzel, F. Hauptert, and M. Q. Zhang, *Composites Science and Technology*, **63**, 2055 (2003).